Research article

Scar formation in the presence of mitomycin C and the anti-fibrotic antibody in a rabbit model of glaucoma microsurgery: A pilot study

Aakriti Garg Shukla [a,b], Tatyana Milman [a], Jolanta Fertala [c], Andrzej Steplewski [c], Andrzej Fertala [c,*]

[a] Wills Eye Hospital, Philadelphia, PA, USA
[b] Glaucoma Division, Edward S. Harkness Eye Institute, Columbia University Irving Medical Center, New York, NY, USA
[c] Department of Orthopaedic Surgery, Sidney Kimmel Medical College, Thomas Jefferson University, Philadelphia, PA, USA

ABSTRACT

Purpose: This study aimed to evaluate the utility of a rationally engineered antibody that directly blocks collagen fibrillogenesis to reduce scar tissue formation associated with subconjunctival glaucoma surgery.

Material and methods: Fourteen eyes of 7 adult rabbits underwent glaucoma filtering surgery using XEN 45 Gel Stent. The rabbits' eyes were divided randomly into three treatment groups: (i) treated with the antibody, (ii) treated with mitomycin C, and (iii) treated with the antibody and mitomycin C. Following surgeries, the intraocular pressure and bleb appearance were evaluated in vivo. The rabbits were sacrificed 8 weeks after the surgery, and their eyes were harvested and processed for tissue analysis. Subsequently, tissue samples were analyzed microscopically for fibrotic tissue and cellular markers of inflammation. Moreover, the collagen-rich fibrotic tissue formed around the stents was analyzed using quantitative histology and infrared spectroscopy. The outcomes of this study were analyzed using the ANOVA test.

Results: This study demonstrated no significant differences in intraocular pressure, bleb appearance, or presence of complications such as bleb leak among the treatment groups. In contrast, we observed significant differences among the subpopulations of collagen fibrils formed within scar neo-tissue. Based on the spectroscopic analyses, we determined that the relative content of mature collagen cross-links in the antibody-treated group was significantly reduced compared to other groups.

Conclusions: Direct blocking of collagen fibrillogenesis with the anti-collagen antibody offers potentially beneficial effects that may reduce the negative impact of the subconjunctival scarring associated with glaucoma filtering surgery.

1. Introduction

Glaucoma is the most common cause of irreversible blindness globally. Over 111 million people will have glaucoma by 2040 [1].

---

* Corresponding author. Department of Orthopaedic Surgery; Sidney Kimmel Medical College, Thomas Jefferson University; Curtis Building, Room 501, 1015 Walnut Street, Philadelphia, 19107, PA, USA.
  E-mail address: axf116@jefferson.edu (A. Fertala).

Lowering intraocular pressure (IOP) remains the only modifiable risk factor for glaucoma, and subconjunctival filtering surgery to create an accessory aqueous outflow channel is the mainstay of accomplishing this goal [2]. Options for filtering surgery have expanded from trabeculectomy and tube shunt surgery to minimally invasive glaucoma surgeries, including the XEN 45 Gel Stent (Abbvie, Inc; Irvine, CA) [3], which is fabricated from porcine collagen molded into a tube. However, scar tissue can form around it after implanting the stent, altering its function, deforming its shape, and blocking the outlet. Furthermore, fibrosis can change the morphology and permeability of the bleb surrounding the stent [4].

Bleb failure in filtering surgery remains an issue. Despite using standard-of-care anti-scarring agents, 50% of glaucoma filtering surgery fails due to scarring of the outflow channel within 5 years postoperatively, with 30% requiring re-operation [5]. Mitomycin C (MMC) is applied in the subconjunctival space during surgery to minimize bleb failure and extend the IOP-reducing effects of trabeculectomy. This anti-proliferative agent targets the fibroblasts responsible for producing scar tissue. Although MMC reduces scar formation, bleb failure is a common outcome despite its use [5]. Using MMC also carries the risk of significant side effects, including conjunctival epithelium breakdown, hypotony, and endophthalmitis [6–9]. Consequently, effective and safe adjuncts to glaucoma filtering surgery that prevent the excessive deposition of collagen-rich scar tissue would potentially reduce or inhibit channel blockage, thus reducing the need for repeat surgeries.

Our group hypothesizes that scar formation and bleb failure can be reduced by directly blocking the assembly of collagen fibrils that form scar tissue [10,11]. Consequently, this pilot study sought to compare the clinical benchmark, *i.e.,* MMC, against the anti-collagen I antibody (ACA) that targets the C-terminal telopeptide of the α2(I) chain and reduces collagen fibrillogenesis to determine their effectiveness in preventing subconjunctival scarring associated with glaucoma filtering surgery [10–12].

We employed a rabbit-based model of bleb-producing glaucoma surgery to test the ACA's efficacy in reducing the associated scarring. We compared the anti-scarring properties of the ACA with those of MMC. The results of our pilot study provide new information on the potential and limitations of the ACA-based inhibitors of ocular fibrosis.

2. Methods

2.1. ACA preparation

Recombinant ACA was expressed in Chinese hamster ovary (CHO) cells cultured in a bioreactor [13]. The ACA was purified by affinity chromatography and then sterilized by filtration [10,11].

2.2. Surgical procedure

Seven New Zealand White rabbits (3 males and 4 females) between 8 and 12 months old were employed to test the ACA's utility to limit the scar formation around the XEN 45 Gel Stents. The rabbits' eyes were divided into the following groups: (i) treated only with ACA (number of eyes = 5), (ii) treated only with MMC (number of eyes = 4), and (iii) treated with ACA and MMC (number of eyes = 5).

The Institutional Animal Care and Use Committee of Thomas Jefferson University reviewed and approved the study protocol. All animals were treated under the Association of Research in Vision and Ophthalmology Statement for the Use of Animals in Ophthalmic and Vision Research.

2.3. Surgical procedure

All procedures were performed by an American Glaucoma Society (AGS) fellowship-trained glaucoma specialist who was masked to the treatment group. Following general anesthesia, topical proparacaine 1% and povidone-iodine 5% were administered to the eye and allowed to dry for 2 min. Then, lidocaine gel 1% was applied to the eye for 2 min. Subsequently, a lid speculum was used to open the eye. XEN 45 Gel Stent (a generous gift from Allergan, Dublin, Ireland) surgery was performed with an *ab externo* approach. The *ab externo* approach was selected due to many potential benefits, including the lack of need for corneal incisions, intraocular maneuvers that could potentially lead to tissue damage in the shallow anterior chamber of the rabbit eye, and the need for viscoelastic material, minimizing the risk of postoperative IOP spike.

In brief, a 7-0 vicryl suture on a tapered needle was passed through half the thickness of the superior peripheral cornea. This traction suture allowed for excellent conjunctival exposure and counter traction. The point of conjunctival entry was 5 mm posterior to the limbus, and the scleral entry point was placed 2 mm posterior to the limbus. Calipers were used to mark 2 mm and 5 mm. Next, non-toothed forceps were used to lift the conjunctiva 5 mm posterior to the limbus. The XEN injector needle was introduced into the subconjunctival space and toward the limbus. Care was taken to avoid perforation through the conjunctiva and vascular regions. The injector system entered the sclera 2 mm posterior to the limbus.

A scleral track was created with counter-traction from the traction suture. The needle was advanced until the tip was visualized in the anterior chamber; the counter-traction was then released, and the XEN 45 Gel Stent was deployed. The implant length in the anterior chamber and the subconjunctival space was confirmed and adjusted with nontoothed forceps as needed, with a goal of approximately 1 mm in the anterior chamber, 2 mm in the scleral tunnel, and 3 mm in the subconjunctiva. Subsequently, the bleb formation was visualized and documented. Injections of ACA alone, MMC (Fagron Sterile Services, Wichita, KS) alone, and MMC and ACA (more detail provided below) as per the randomization scheme were performed adjacent to the bleb intraoperatively.

The region was checked for Seidel positivity with fluorescein strips and blue light. Subsequently, ofloxacin and prednisone acetate were administered to the eye's surface at the case's conclusion. After recovering from anesthesia, the rabbits were returned to their

pans.

2.3.1. Intraoperative and postoperative ACA and MMC injections

In the first group, referred to as the ACA group, ACA was administered intraoperatively (POD0), postoperatively a week later (POW1), and then, at POW2, POW3, POW6, and POW8 by injecting 1.5 mg of the antibody in 50 μl of phosphate-buffered saline (PBS). In the second group, specified as the MMC group, a 50-μl dose, at the concentration of 0.2 mg/ml, was administered only once intraoperatively. In the postoperative period, although no MMC injections were performed, sham injections of 50 μl of PBS were injected at the same frequency as ACA injections in the ACA group, at POW1, POW2, POW3, POW6, and POW8.

We chose MMC at 0.2 mg/ml over 0.4 mg/ml, as prior studies in rabbits have shown desired effects with lower concentrations. Furthermore, human studies suggested lower rates of complications, such as bleb leak and hypotony, with a lower concentration of MMC [14,15].

The third group, referred to as the ACA/MMC, was treated with the ACA and MMC. MMC was administered only once in this group by injecting a 50-μl dose, at 0.2 mg/ml, during surgery. In the same group, ACA was administered POD0, then at POW1, POW2, POW3, POW6, and POW8 at the same concentration as in the ACA-only group (see above).

2.3.2. Clinical Assessment

Animals were examined preoperatively on the day of surgery, on postoperative day 1 (POD1), then POW1, POW2, POW3, POW6, and POW8. Each time, the IOP was measured twice using a tonometer (ICare TONOVET Plus, iCare Finland, Vantaa, Finland) by an AGS specialist who was masked to the treatment. Care was taken to ensure that rabbits were not under stress while IOP was checked. Preoperatively and postoperatively at POW1, POW2, POW3, POW6, and POW8, eyes were examined under a microscope to assess the Seidel positivity and the position of the stent.

Results from the IOP measurements were presented graphically, considering the preoperative IOP 100%. The statistical significance of the IOP differences measured among the ACA, MMC, and ACA/MMC treatments was analyzed using repeated-measures ANOVA (IBM SPSS Statistic for Windows, version 26, IBM Corp., Armonk, NY). In all assays, statistical significance was defined as $p \leq 0.05$.

2.3.3. Tissue collection

Following euthanasia, the position of the stents was marked with nylon sutures. Then, the rabbits' eyes were enucleated and placed into 4% paraformaldehyde. Each eye was examined under the dissecting microscope, and the site of the orienting suture was marked. The anterior segment of the eye was removed by opening the eye equatorially. A central cross-section of the anterior segment was taken in the plane to incorporate the stent. The remaining anterior segment tissues were radially sectioned perpendicular to the limbus.

Following routine tissue processing and paraffin embedding, each block was sectioned in three-step levels at 50-μm intervals. Five 5-μm thick sections were obtained at each level; two were stained with hematoxylin-eosin (H&E) and periodic acid-Schiff stains. The remaining unstained preparations were used for histological assays of collagen fibrils stained with picrosirius red.

2.3.4. Histopathology of the eyes

H&E-stained sections were analyzed in a blinded fashion by an ocular pathologist (TM), who assessed the anterior segment tissues for stent location, the presence of inflammatory cells, and the extent of fibrosis in the stent area. Based on these analyses, we determined the percentage of samples in which fibrotic deposits were readily visible. In total, we analyzed 119 slides representing different levels of collected tissues. On average, we analyzed 8.5 slides/eye.

2.3.5. Histological assays of collagen fibrils

Since the scar tissue comprises collagen fibrils predominantly, the ocular tissues were stained with collagen-specific picrosirius red dye [16,17]. Combining this staining technique with polarized-light microscopy makes it possible to approximate fibrils' thickness, organization, and packing density [16,18–20]. Studies have determined that as the thickness of fibers increases, their birefringence color changes under the polarized light microscope from green to yellow to orange to red, *i.e.*, from shorter to longer optical wavelengths [16,21–24].

Here, the focus of the quantitative assays was thin green-birefringence fibrils. Research demonstrated that the relative content of these fibrils increases during the scar formation process [25]. Hence, quantifying the relative content of these fibrils provides a reliable method to determine the extent of the formation of collagen-rich scar neo-tissue. Moreover, measuring the relative content of these fibrils as the function of an anti-fibrotic treatment helps to determine the utility of tested anti-fibrotic agents to modulate the collagen content directly in a target tissue.

Employing a polarizing microscope (Eclipse LV100POL, Nikon Inc., Melville NY) and the NIS Elements software (Nikon Inc.), the following groups of the birefringence colors were defined in captured images: (i) green birefringence (GB; identifies thin, loosely packed fibrils), (ii) yellow birefringence (YB; identifies intermediate-thickness fibrils), and (iii) red birefringence (RB; identifies thick, tightly packed fibrils) [13,18].

All fibrils in the viewing areas were analyzed according to described methods [17,18]. In brief, the birefringence colors were delineated by utilizing the software's color threshold function. Then, the software determined the percentages of the areas occupied by the pixels corresponding to the specified colors. Eight regions of interest (ROIs) per a rabbit-derived tissue sample were analyzed, and the data were averaged.

Subsequently, we applied one-way ANOVA to determine the statistical significance of differences among studied groups. Using this method, we measured the differences in the relative content of the GB fibrils in the conjunctiva and sclera regions surrounding the

implants as the function of applied treatment (IBM SPSS Statistic for Windows, version 26). In addition, we analyzed corresponding regions present in non-injured areas of the eyes.

Moreover, results on the relative content of the RB-fibrils and YB-fibrils were also presented in a graphic form (OriginPro version 2023, OriginLab Corporation, Northampton, MA).

2.3.6. Fourier transform infrared spectroscopy (FTIR)-based assays of the collagen content and cross-links

In biological studies, FTIR spectroscopy utilizes infrared light to analyze the chemical composition of tissue materials [26]. Here, we applied FTIR to study the collagen content and the extent of cross-linking collagenous materials forming the conjunctiva and sclera structures following glaucoma surgery.

A crucial advantage of FTIR spectroscopy-based assays over histological and biochemical methods is that they are non-destructive on intact, label-free tissue samples. Consequently, FTIR spectroscopy of tissues provides quantitative information about analyzed molecules in the context of their spatial arrangement and position within ocular tissues [27].

Methodological principles of FTIR tissue assays are based on generating spectral images derived from molecular vibrations of molecular bonds subjected to the IR beam. Many tissue macromolecules, including collagens, have unique spectral signatures that allow the quantification of these molecules in ocular tissues [28,29].

Here, we used this method to compare the relative collagen content in the scar tissues formed around the implants as the function of the anti-scarring treatment. Utilizing generated spectra, we determined the surface areas of the collagen-specific peaks (arising due to CH_2 wagging vibrations of proline side chains) centered around 1338 cm^{-1} wavenumber. We utilized the surface area of a protein-specific amide II peak (arising from N–H bending vibration) centered around 1550 cm^{-1} wavenumber as an internal reference representing a total protein content. Consequently, the collagen/amide II ratios were measured to determine the relative collagen content [11,30,31]. Hence, the bigger the ratio values, the greater the relative collagen content.

Since the extent of collagen cross-linking within the fibrillar structures determines the scars' maturity, we utilized FTIR to study the cross-linking status of collagen matrices formed in response to stent implantation. In particular, we measured the pyridinoline (PYR) peak, representing mature collagen cross-links (centered around 1660 cm^{-1}) and dehydro-dihydroxynorleucine (de-DHLNL), representing immature cross-links (centered around 1690 cm^{-1} wavenumber) [11,32,33]. Hence, the maturity of the collagen fibrils' cross-links was defined as the PYR/de-DHLNL ratio; high ratios indicated a relatively high amount of mature cross-links, while low ratios indicated lower levels of mature cross-links. Studies demonstrated that this ratio increases during many fibrotic processes [34–36]. Consequently, in situ assays of the PYR/de-DHLNL ratios provides a relevant parameter to evaluate the fibrotic status of the collagen-rich neo-tissues formed in the presence of anti-scarring agents analyzed here.

Paraffin-embedded 5-μm thick tissue sections were deposited on the MirrIR low-e microscope slides (Kevley Technologies, Chesterland, OH). An FTIR spectrometer (Spotlight 400, PerkinElmer, Waltman, MA) was used to analyze the ROIs in the eyes' conjunctivae and sclerae. The measurements were done in the 4000 cm^{-1} to 748 cm^{-1} wavenumbers spectral range, at a pixel resolution of 50 μm, 8 scans per pixel, and a spectral resolution of 4 cm^{-1}. The Spectrum Image software generated co-added spectra from scanned ROIs (PerkinElmer, Inc.). On average, we collected the infrared spectra from 3 ROIs/eye.

Overlapping peaks of the FTIR-derived spectra were deconvoluted and analyzed based on the second-order derivative spectra and pre-determined bell-type Gaussian peak fitting function using the OriginPro software (OriginPro version 2021) [11,37,38].

One-way ANOVA was conducted to determine the significance of the difference in measured parameters among treatment groups (IBM SPSS Statistic for Windows, version 26). In all assays, statistical significance was defined as $p \leq 0.05$.

Results on the relative collagen content and the cross-links were also presented as box plots (OriginPro, version 2023).
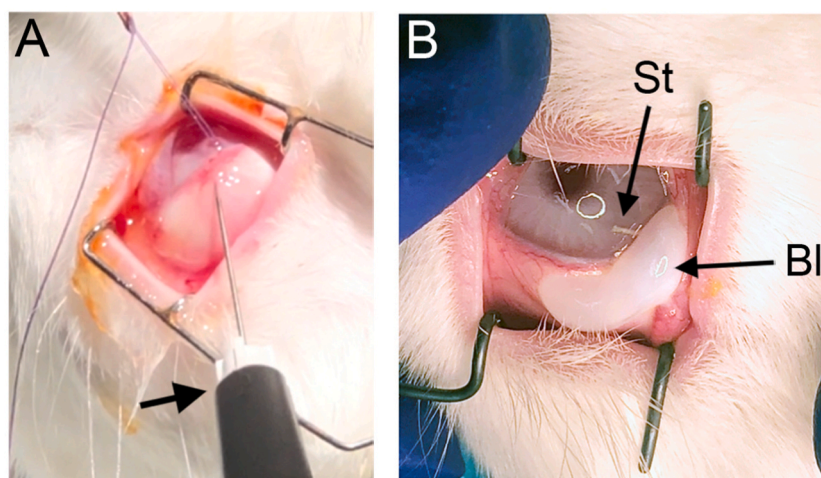

Fig. 1. A, Implantation of the XEN 45 Gel Stent into the rabbit eye using a stent applicator (arrow). B, A photograph of the stent (St) position and the bleb (Bl) morphology.

3. Results

3.1. Animal model

All animals underwent bilateral placement of XEN 45 Gel Stents. Surgery and the postoperative course were well tolerated (Fig. 1 A & B). All eyes remained Seidel negative throughout the postoperative follow-up period. Moreover, we observed neither local nor systemic adverse reactions to the ACA. In 1 of 7 rabbits randomized to MMC in the right eye and ACA/MMC in the left eye, significant conjunctival injection and chemosis were noted bilaterally. This issue resolved spontaneously without the need for any treatment. All eyes were utilized for in-life IOP assays and experiments on collected ocular sections.

3.2. IOP measurements

Repeated between-the-subjects measures ANOVA demonstrated that there were no statistically significant differences in the IOP among the ACA, MMC, and ACA/MMC treatment groups ($F(2, 11) = 1.5$, $p = 0.266$) (Fig. 2).

3.3. Histopathology

In each eye, we analyzed injured sites at implantation of the stents and uninjured sites located 180° from the implants (Fig. 3 A). As indicated in Fig. 3 A, all uninjured sites had a normal appearance. The presence of fine collagen fibrils characterized their conjunctivas (Fig. 3 B) and thicker fibrils were observed in the sclerea (Fig. 3C). Sparse, spindle-shaped fibroblasts were arranged regularly in the collagenous fibrillar structure (Fig. 4).

Following tissue processing, XEN 45 Gel Stent implants (Fig. 3 A & D) were identified in 3 eyes (2 in the anterior chamber and adjacent cornea/subconjunctival space, and 1 in the cornea). Although the actual implants in the histological sections were not always readily visible, we identified the sites of the implants by the presence of distinct voids and scar-like tissues around them (Figs. 3 A & 5 B). Except for one eye from the ACA-treated group, there was a prominent inflammatory infiltrate (Fig. 5 A & B). In the regions of the stent placement in all experimental groups, this infiltrate consisted of a variable proportion of lymphocytes, plasma cells, neutrophils, and eosinophils seen in the anterior segment tissues, i.e., conjunctiva, episclera, sclera, cornea, trabecular meshwork, extraocular muscle, and ciliary body (Fig. 5 A & B). Notably, unlike the MMC and ACA/MMC groups, we did not observe inflammatory cells in the ACA-treated group's ciliary body region. Fig. 5 A & B demonstrates inflammatory cells present in representative regions of conjunctivas from the ACA/MMC group.

Moreover, we observed morphologic evidence of fibrosis in all analyzed groups based on the appearance of the fibroblastic cells and fibrillar structures seen in H&E-stained tissue slices (Fig. 5 A & B). In 42 samples collected from various tissue levels of the ACA group, we observed fibrotic morphological features in 6 samples (14.3%). In 33 tissue samples collected from the MMC group, similar features were observed in 3 (9.1%). In 44 samples from the ACA/MMC group, morphological fibrotic features were observed in 23 tissue slices (52.3%).

Variable degrees of fibrosis and granulation were also observed in all treatment groups. In one case, a foreign-body-type inflammatory response was associated with the stent (Fig. 5 B). In contrast, the anterior segment structures distant from the site of stent placement lacked inflammation, granulation tissue, and fibrosis (Fig. 3 A).

3.4. Collagen fibrils

Analysis of the relative content of specific birefringence subpopulations (Fig. 6A–C) of collagen fibrils formed around the implant (injured sites) within the conjunctivae demonstrated a significant difference in the GB fibrils content among various treatment groups
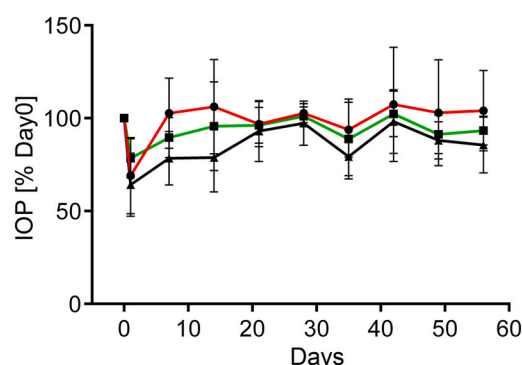

Fig. 2. A graphic representation of the intraocular pressure (IOP) values measured on the indicated postoperative days. Data points ($\pm$ standard deviations; SD) indicate the IOP changes expressed as the percent values of the IOP measured preoperatively (considered 100%). Data from the ACA-treated (●), MMC-treated (■), and ACA/MMC-treated (▲) eyes are presented.
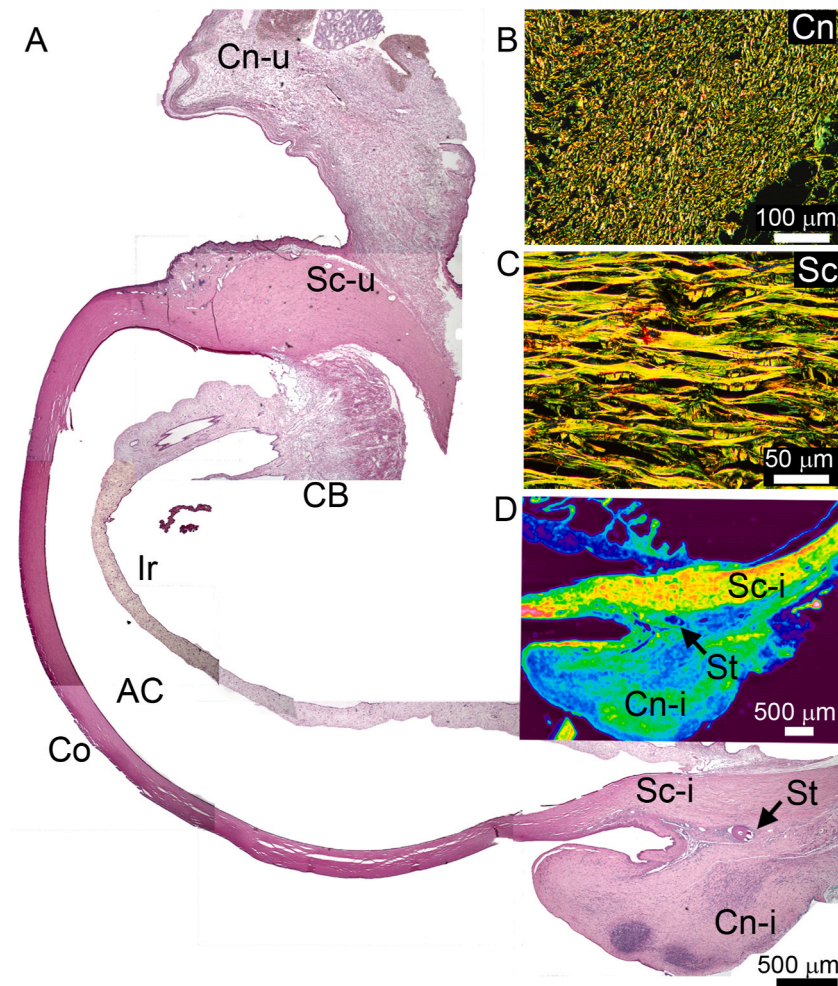
Fig. 3. Representative images of ocular tissues analyzed with microscopic and spectral techniques. A general view of the cross-section of the rabbit's eye (A). Picrosirius staining of the conjunctiva (B). Picrosirius staining of the sclera (C). An FTIR spectroscopy map shows an average absorbance at the depicted area (D). Symbols: Cn-u, Cn-i; conjunctiva regions present at the injured (i) and uninjured (u) sites, Sc-u, Sc–I; sclera regions present at injured (i) and uninjured (u) sites, Co; cornea, CB; ciliary body, Ir; iris. Arrows indicate the stent (St).

(Fig. 6C) ($F(2, 11) = 8.881$, $p = 0.005$). Post-hoc analysis showed that this difference was contributed to by a significant reduction in the GB fibrils in the ACA group vs. ACA/MMC group ($p = 0.006$) and MMC group vs. ACA/MMC group ($p = 0.003$). There was no statistical difference between the ACA and MMC groups ($p = 0.523$).

Similar assays of the injured sites done in the sclerae (Fig. 7A–C) did not show any significant differences in the content of the GB fibrils present in the ACA, MMC, and ACA/MMC groups ($F(2, 11) = 1.24$, $p = 0.327$) (Fig. 7C).

Analyses of the relative content of the thin GB collagen fibrils in uninjured sites demonstrated no significant differences among the ACA, MMC, and ACA/MMC groups (Figs. 6 D-F & 7 D-F). The differences were observed neither in the conjunctiva regions (Fig. 6D–F) ($F(2, 11) = 0.944$, $p = 0.418$) nor the sclera regions ($F(2, 11) = 0.703$, $p = 0.516$) (Fig. 7D–F).

3.5. FTIR assays of relative collagen content

FTIR spectra were collected and analyzed using the OriginLab peak fitting function (Fig. 8 A). The fit was appropriate, as indicated by symmetrically distributed residuals seen in Fig. 8 B.

The collagen changes were measured relative to the total protein content represented by the amide II peak (Fig. 9 A & B). Based on the analyses of the injured sites, we observed no significant differences in the relative collagen content among the ACA, MMC, and ACA/MMC treatment groups. We observed differences neither in the conjunctivae regions ($F(2, 11) = 0.458$, $p = 0.644$) (Fig. 9 A) nor in the sclerae regions ($F(2, 11) = 0.939$, $p = 0.42$) (Fig. 9 B).

Considering the injured versus uninjured sites, regardless of the treatment method, we observed a significant decrease in the relative amount of collagen formed in the injured conjunctivas around the shunt versus the collagen amount in the corresponding regions of the uninjured side ($F(1, 26) = 7.158$, $p = 0.013$) (Fig. 10 A). In contrast, there was no difference in the relative collagen
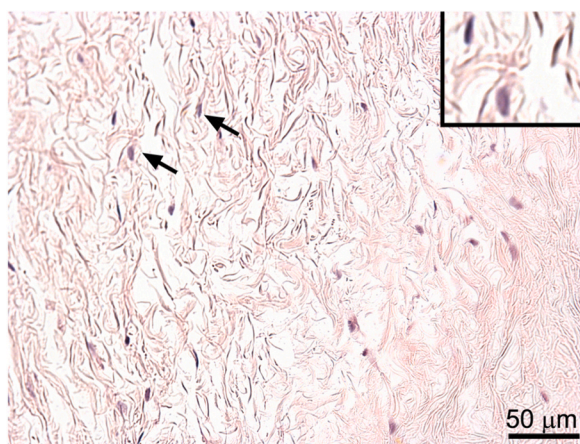
Fig. 4. A representative image of the uninjured conjunctiva site from the ACA/MMC group showing a morphologically unremarkable stroma, containing loosely arranged collagen matrix populated with sparsely arranged fibroblasts (arrows). The insert shows an enlarged detail of the conjunctiva and fibroblasts.
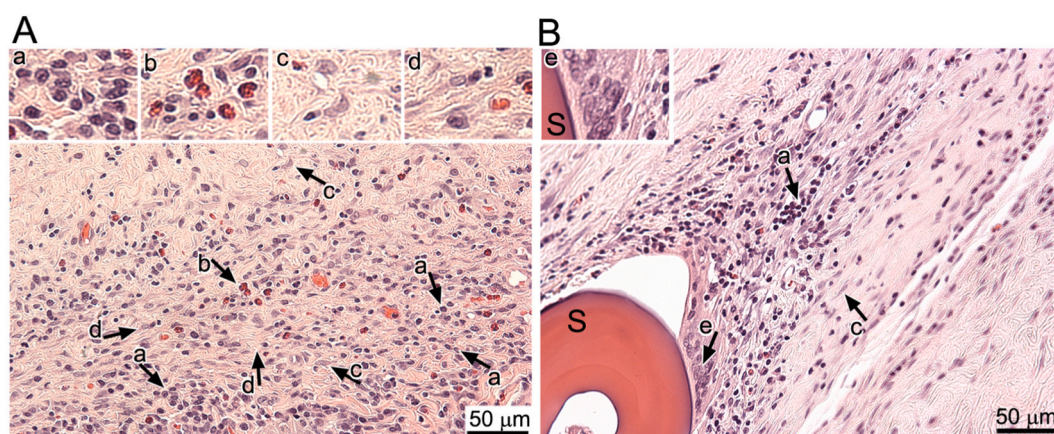

Fig. 5. Histology of the conjunctiva regions from around the stent implanted in a rabbit from the ACA/MMC group. H&E-stained samples (A & B) showing (arrows) intense mixed inflammatory infiltrate comprising groups of lymphocytes, plasma cells, macrophages (a), eosinophils (b), and activated fibroblasts (c) in the background of dense eosinophilic collagen fibrosis (d). Multinucleated giant cells (e) adjacent to the implant (S) were also present (B). Inserts show details of the observed areas (A & B).

amounts in the injured and uninjured sides of sclerae ($F(1, 26) = 0.292$, $p = 0.594$) (Fig. 10 A).

Also, FTIR-based assays of uninjured sites showed no significant differences in the relative collagen content among the ACA, MMC, and ACA/MMC treatment groups. We observed differences in neither the conjunctivae regions ($F(2, 11) = 0.913$, $p = 0.43$) nor in the sclerae regions ($F(2, 11) = 1.317$, $p = 0.307$) (Fig. 11 A).

3.6. FTIR assays of collagen cross-links

In the conjunctivae regions adjoining the implants, FTIR-based assays of the PYR/de-DHLNL ratios indicated significant differences in the relative content of mature collagen cross-links among the treatment groups ($F(2, 11) = 38.064$, $p < 0.0001$) (Fig. 9C). A post hoc analysis showed that this difference was contributed to by significantly reducing the PYR/de-DHLNL ratio in the ACA group vs. MMC group ($p < 0.0001$) and ACA group vs. ACA/MMC group ($p < 0.0001$). There was no statistically significant difference between the MMC and ACA/MMC groups ($p = 0.00.09$).

Similarly, we observed significant differences in the PYR/de-DHLNL ratios among the injured sclerae regions of the ACA, MMC, and ACA/MMC groups ($F(2, 11) = 6.427$, $p = 0.014$) (Fig. 9 D). A post hoc analysis indicated that this difference was contributed to by significantly reducing the PYR/de-DHLNL ratio in the ACA group vs. MMC group ($p = 0.08$), decreasing this ratio in the ACA/MMC group vs. MMC group ($p = 0.011$). There was no statistically significant difference between the ACA and ACA/MMC groups ($p = 0.859$).

Comparison of the PYR/de-DHLNL in the injured conjunctiva sites vs. uninjured sites in all rabbits, regardless of the treatment
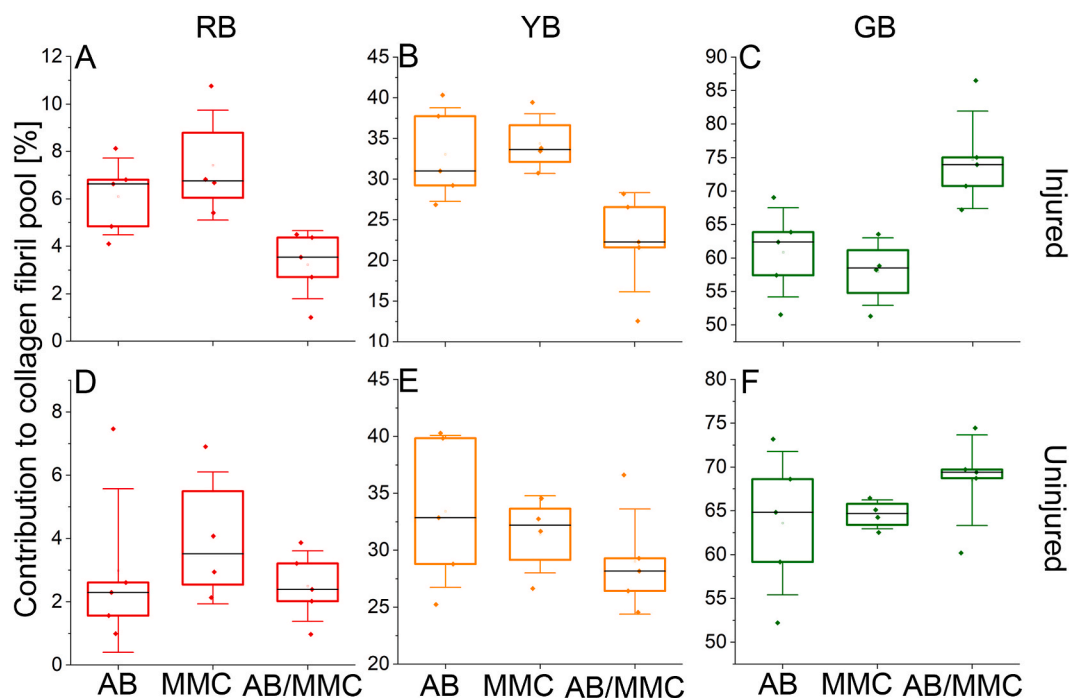
Fig. 6. Box plots of relative amounts of RB (A & D), YB (B & E), and GB (C & F) collagen fibrils in injured (A–C) and uninjured (D–F) regions of conjunctivas. Separate boxes describe data for the ACA, MMC, and ACA/MMC groups. The interquartile range between the 25th and 75th percentiles determines each box. The lines within the boxes represent the medians, while the whiskers delineate the SD values.
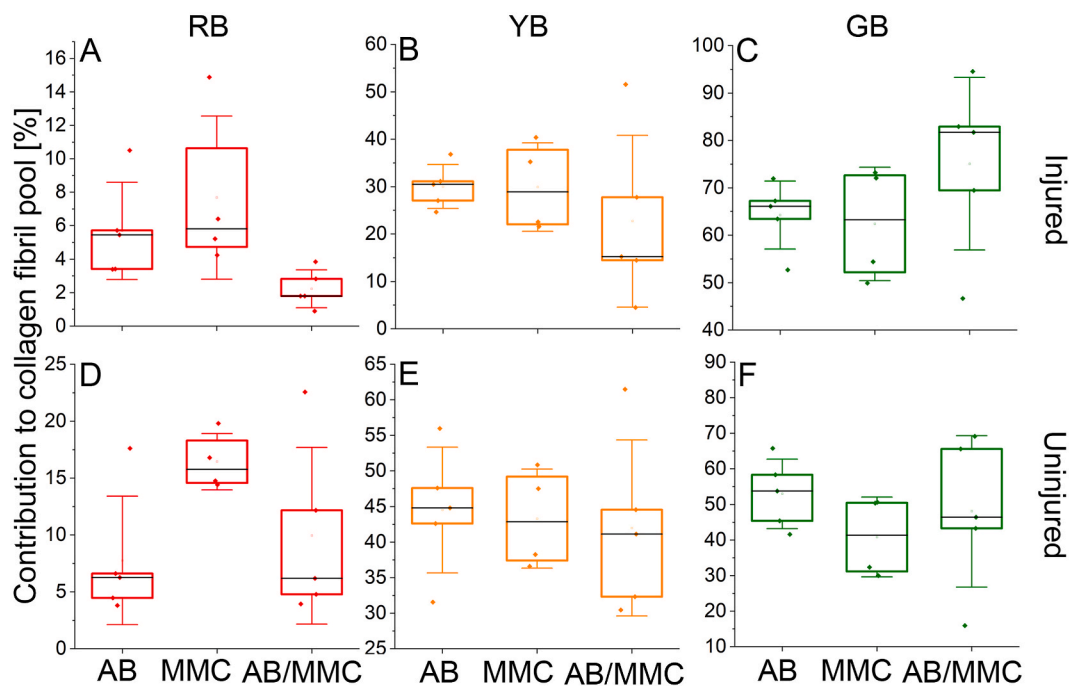

Fig. 7. Box-plot representations of relative amounts of RB (A & D), YB (B & E), and GB (C & F) collagen fibrils in injured (A–C) and uninjured (D–F) regions of sclerae. Separate boxes illustrate data for the ACA, MMC, and ACA/MMC groups. The interquartile range between the 25th and 75th percentiles determines each box. The lines within the boxes represent the medians, while the whiskers delineate the SD values.
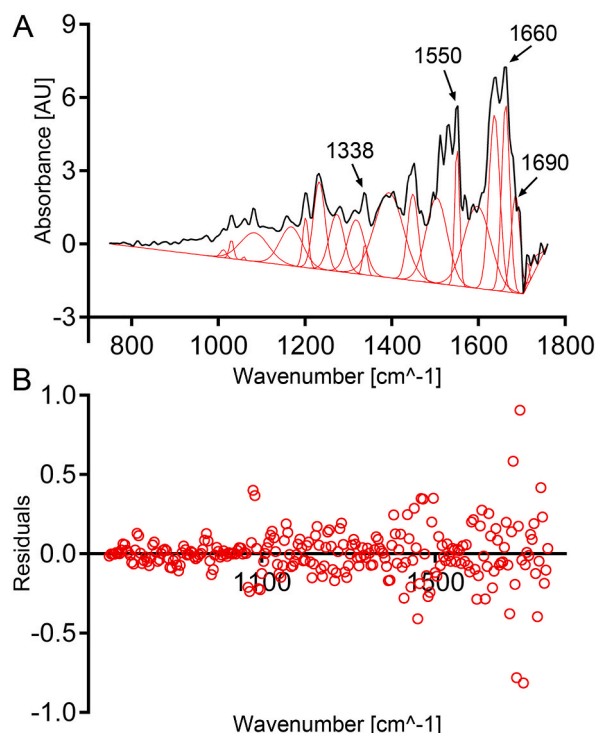
Fig. 8. An example of a representative fitted FTIR spectrum (A) collected from analyzed ocular tissues. Corresponding residuals, i.e., the differences between the response data and the fit to the response data at each predictor value, indicating a proper fit, are also presented (B). Spectral peaks utilized in this study are marked with arrows.

mode, indicated an increase of this ratio in the injured regions (Fig. 10 B). This difference was not statistically significant ($F(1, 26) = 0.069$, $p = 0.795$). A similar increase was observed in the injured and uninjured sclera regions ($F(1, 26) = 1.716$, $p = 0.202$) (Fig. 10 B).

Also, FTIR-based assays of uninjured sites showed no significant differences in the PYR/de-DHLNL ratios among the ACA, MMC, and ACA/MMC treatment groups. No differences were observed in this ratio in either the conjunctivae regions ($F(2, 11) = 1.244$, $p = 0.326$) (Fig. 11C) or the sclerae regions ($F(2, 11) = 2.032$, $p = 0.177$) (Fig. 11 D).

4. Discussion

Although current clinical practice often utilizes MMC as an anti-scarring agent during subconjunctival glaucoma surgeries, this agent is associated with adverse effects. Furthermore, the long-term effects of using MMC remain controversial. For instance, after analyzing 698 participants who underwent trabeculectomy, Wilkins et al. concluded that MMC treatment reduced mean IOP and appeared to reduce the relative risk of trabeculectomy failure in analyzed patients [39]. In a more recent study, Foo et al. analyzed the effectiveness and safety of MMC versus no MMC used during aqueous shunt surgery to reduce IOP in 333 primary and secondary glaucoma patients. The authors did not see any strong evidence that MMC treatment reduced IOP 12 months post-surgery compared to placebo [40].

In the study presented here, we employed a rabbit-based model to analyze the utility of the antibody that blocks collagen fibril-logenesis to reduce postoperative scar tissue formation around the XEN Gel Stent. In our earlier studies, we demonstrated the utility of the antibody in limiting excessive scarring in arthrofibrosis, keloid, and lung fibrosis models [11,13,41].

In the model employed here, we observed scar neo-tissue formed around the stents, regardless of the treatment we applied. However, these scars did not cause any significant changes in the IOP values measured in the rabbits treated with ACA, MMC, or ACA/MMC. It is likely that in future tests, it will be necessary to induce ocular hypertension in our animal model using, for example, photocoagulation of the trabecular meshwork, cauterization of the episcleral veins, or topical steroid application to measure any IOP-reducing effects of the analyzed compounds [42]. Furthermore, a more extended postoperative period may be needed to allow for more robust scar formation.

Although the scar neo-tissue that formed for 8 weeks around the stents did not impact the IOP, we observed a few significant differences in the composition and structure of the conjunctiva's collagenous material that forms the bulk of the scar neo-tissue. First, we observed fewer GB fibrils in the ACA and MMC groups compared to the ACA/MMC group. As the GB fibrils in the healing tissues represent newly synthesized thin fibrils before they aggregate laterally into thick fibers, we interpret this result as the inhibition of neo-fibrillogenesis by ACA and MMC. We propose, however, that mechanisms of GB fibril reduction differ in the ACA and MMC groups.

In the ACA group, the reduction of the newly synthesized fibrils was most likely due to the antibody-mediated blockage of collagen-
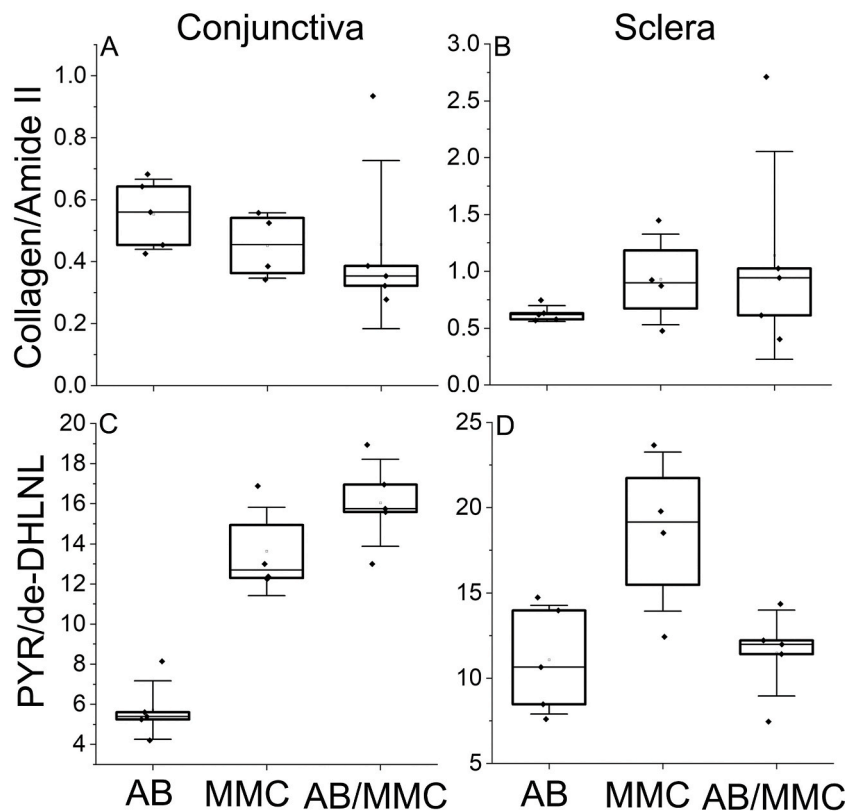
Fig. 9. Analyses the relative collagen and mature cross-linking contents in conjunctivas (A & C) and sclerae (B & D) from injured regions. Box plots of relative amounts of collagens, represented by the collagen peak (centered around 1338 cm^{-1} wavenumber)/amide II peak (centered around 1550 cm^{-1} wavenumber) ratios (A & B). The higher the collagen/amide II ratio, the higher the relative collagen content. Box plots illustrating the maturity of collagen cross-links (C & D). The cross-link maturity is defined as the PYR peak (centered around 1660 cm^{-1} wavenumber)/deDHLNL peak (centered around 1690 cm^{-1} wavenumber) ratio. The higher the PYR/deDHLNL ratio, the greater the maturity of collagen cross-links. Separate boxes illustrate data for the ACA, MMC, and ACA/MMC groups. The interquartile range between the 25th and 75th percentiles determines each box. The lines within the boxes represent the medians, while the whiskers delineate the SD values.

collagen interaction that drives fibril assembly [10]. In the MMC group, this reduction was likely due to blocking cell proliferation, which ultimately reduced overall collagen production.

We observed no cumulative effects of the ACA/MMC treatment. Indeed, the ACA/MMC group contained a more significant amount of GB fibrils compared to other groups. We expect, however, that MMC likely binds to the antibody, reducing both interactants' potency. Documented binding of MMC to serum proteins via hydrophobic interaction supports this notion [43].

Of note was the FTIR-based observation that there was no statistically significant difference among the ACA, MMC, and ACA/MMC groups in the relative amounts of total collagen deposited in the scar tissue formed in the conjunctivae and sclerae around the shunt.

However, we observed a decrease in relative collagen content when we compared the injured vs. uninjured conjunctiva regions in combined treatment groups. No similar decrease was observed in the corresponding sclerae. These observations suggest that in the rabbit model of glaucoma filtering surgery with the XEN Gel Stent, there is no rapid buildup of the scar neo-tissue's elements, most notably collagenous proteins. We propose that more extended follow-up periods and increased intraocular pressure may be needed to observe more robust changes in the rabbit model.

FTIR-based studies, however, indicated significant differences in the cross-linking patterns of collagen fibrils formed in the conjunctivae scars' neo-tissue. As collagen cross-linking defines the strength and stiffness of collagen fibrils in healthy conditions, an increase in collagen cross-linking is a hallmark of fibrotic scarring [34,35,44–46]. In this study, a significantly smaller PYR/de-DHLNL ratio observed in the ACA group versus MMC and ACA/MMC groups indicates a relatively higher content of immature de-DHLNL cross-links. Given that we also observed a smaller number of thin GB fibrils in the ACA group, we propose that the somewhat higher content of immature cross-links may result from increased cross-link density per fibril unit or delayed cross-link maturation into the PYR form.

Since mature collagen cross-links are the main contributor to tissue stiffness, we propose that the net effect of the reduced content of mature PYR cross-links would be softer scar tissue formed around the stents in the ACA-treated rabbits [46]. The stiff, collagen-rich extracellular matrix (ECM) acts as a crucial pro-fibrotic stimulant of fibroblasts and inflammatory cells [47–49]. Consequently, targeting the formation of stiff ECM with the antibody described here could provide an auxiliary anti-fibrotic approach to limit scarring
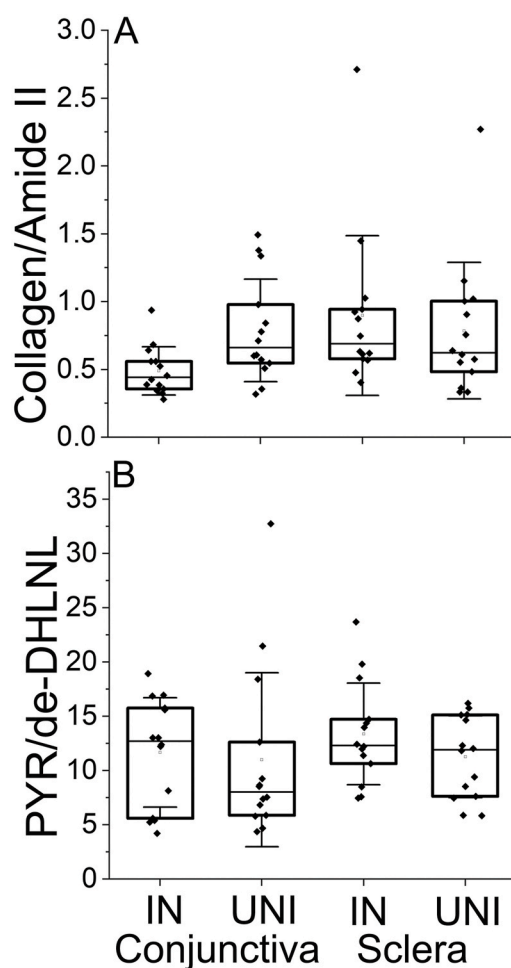
Fig. 10. Analysis of the relative collagen content (A) and cross-links (B) in conjunctivas and sclerae from the injured and uninjured regions. Here, we compared these parameters in the injured and uninjured sites without considering the treatment groups. Box plots of relative amounts of collagens (A), represented by the collagen peak (centered around 1338 cm^{-1} wavenumber)/amide II peak (centered around 1550 cm^{-1} wavenumber)/ratios. The higher the collagen/amide II ratio, the higher the relative collagen content. Box plots illustrating the maturity of collagen cross-links (B). The cross-link maturity is defined as the PYR peak (centered around 1660 cm^{-1} wavenumber)/deDHLNL peak (centered around 1690 cm^{-1} wavenumber) ratio. The higher the PYR/deDHLNL ratio, the greater the maturity of collagen cross-links. Separate boxes illustrate data for the ACA, MMC, and ACA/MMC groups. The interquartile range between the 25th and 75th percentiles determines each box. The lines within the boxes represent the medians, while the whiskers delineate the SD values.

from glaucoma surgeries.

5. Limitations

This study has a few limitations. First, the ACA delivery method we applied here required multiple, direct injections of the antibody. Although this method ensures effective high molecular mass-ACA delivery, it may be associated with unwanted side effects caused by the injury to the injection site. To minimize between-group differences related to potential scarring or injury from postoperative injections, we injected a saline vehicle in the MMC eyes each time the ACA or ACA/MMC eyes underwent ACA injection during the postoperative period. In the future, topical applications or sustained local delivery may provide a safer option for the ACA application. Second, we only studied the rabbit groups for 2 months, which is a relatively short period to expect bleb failure. In future studies, it will be necessary to determine the long-term effects of the ACA treatment on scar formation and subsequent remodeling of the scar tissue. Third, as indicated above, we could not assess the impact of the ACA treatment on the primary treatment's target, *i.e.*, IOP. Hence, an animal model in which the IOP is elevated before the glaucoma surgery is needed to understand the ACA's effects fully. Fourth, except for observing the invasion of inflammatory cells into injury sites, we did not study the biochemical parameters of the inflammatory responses to the XEN Gel Stent presence and their potential pro-fibrotic effects. Fifth, we quantified the collagen and cross-link content in relative terms. For instance, collagen content was presented relative to the overall protein amount. Our system did not allow us to reliably quantify the collagen content in absolute values (e.g., mg of collagen/unit of dry tissue mass). Consequently, we
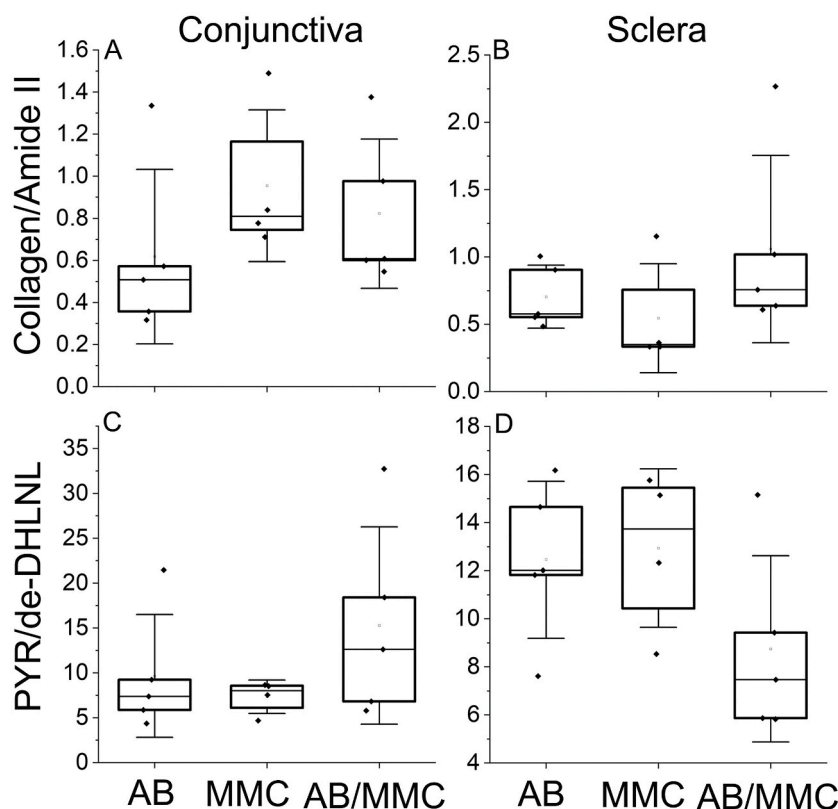
Fig. 11. Analysis of the relative collagen content and the maturity of the cross-linkis in conjunctivas (A & C) and sclerae (B & D) from the uninjured regions. Box plots of relative amounts of collagens, represented by the collagen peak (centered around 1338 cm^{-1} wavenumber)/amide II peak (centered around 1550 cm^{-1} wavenumber) ratios (A & B). The higher the collagen/amide II ratio, the higher the relative collagen content. Box plots illustrating the maturity of collagen cross-links (C & D). The cross-link maturity is defined as the PYR peak (centered around 1660 cm^{-1} wavenumber)/deDHLNL peak (centered around 1690 cm^{-1} wavenumber) ratio. The higher the PYR/deDHLNL ratio, the greater the maturity of collagen cross-links. Separate boxes illustrate data for the ACA, MMC, and ACA/MMC groups. The interquartile range between the 25th and 75th percentiles determines each box. The lines within the boxes represent the medians, while the whiskers delineate the SD values.

cannot state, for example, that in injured ocular tissue, there is more collagen than in non-injured sites. We can only analyze these differences compared to the overall protein content represented by the amide II FTIR peak.

Despite the above limitations, our methods were appropriate to measure the treatment-dependent changes in the collagen parameters and achieve the goals of this study.

6. Conclusion

Our work is the first study analyzing the effects of distinct anti-fibrotic approaches to limit the scar formation around the XEN Gel Stent. This study demonstrated that, in contrast to MMC, the ACA-based system significantly reduces collagen-stabilizing, pro-fibrotic cross-links. Hence, we propose that in the long term, direct targeting of collagen fibrillogenesis may delay and reduce unwanted scarring around glaucoma surgery sites. Additional studies are warranted to address the current research's limitations and better understand the ACA's efficacy in glaucoma filtering surgery.

Author contribution statement

Aakira Garg Shukla; Andrzej Fertala: Conceived and designed the experiments; Performed the experiments; Analyzed and interpreted the data; Contributed reagents, materials, analysis tools or data; Wrote the paper.

Tatyana Milman; Andrzej Steplewski: Performed the experiments; Analyzed and interpreted the data; Contributed reagents, materials, analysis tools or data; Wrote the paper.

Jolanta Fertala: Conceived and designed the experiments; Performed the experiments; Analyzed and interpreted the data; Wrote the paper.

Funding statement

Data availability statement

Data included in article/supplementary material/referenced in article.

Declaration of interest's statement

The authors declare the following conflict of interests: Andrzej Steplewski and Andrzej Fertala are inventors of a patent that protects the sequence of the antibody employed here.

Acknowledgments

References

[1] Y.C. Tham, et al., Global prevalence of glaucoma and projections of glaucoma burden through 2040: a systematic review and meta-analysis, Ophthalmology 121 (11) (2014) 2081–2090.

[2] R. Lim, The surgical management of glaucoma: a review, Clin. Exp. Ophthalmol. 50 (2) (2022) 213–231.

[3] F.A. Birnbaum, C. Neeson, D. Sola-Del Valle, Microinvasive glaucoma surgery: an evidence-based review, Semin. Ophthalmol. 36 (8) (2021) 772–786.

[4] C. Gizzi, et al., Trabeculectomy following failed ab interno gelatin microstent: case series, J. Glaucoma 27 (10) (2018) e168–e173.

[5] S.J. Gedde, et al., Treatment outcomes in the Tube versus Trabeculectomy (TVT) study after five years of follow-up, Am. J. Ophthalmol. 153 (5) (2012) 789–803 e2.

[6] V.P. Costa, et al., Efficacy and safety of adjunctive mitomycin C during Ahmed Glaucoma Valve implantation: a prospective randomized clinical trial, Ophthalmology 111 (6) (2004) 1071–1076.

[7] J.A. Prata Jr., et al., Effects of intraoperative mitomycin-C on the function of Baerveldt glaucoma drainage implants in rabbits, J. Glaucoma 5 (1) (1996) 29–38.

[8] O. Yamanaka, et al., Pathobiology of wound healing after glaucoma filtration surgery, BMC Ophthalmol. 15 (Suppl 1) (2015) 157.

[9] L.F. Seet, et al., Effects of valproic acid and mitomycin C combination therapy in a rabbit model of minimally invasive glaucoma surgery, Trans. Vis. Sci. Tech. 11 (1) (2022) 30.

[10] H.J. Chung, et al., Collagen fibril formation. A new target to limit fibrosis, J. Biol. Chem. 283 (38) (2008) 25879–25886.

[11] A. Steplewski, et al., Mechanisms of reducing joint stiffness by blocking collagen fibrillogenesis in a rabbit model of posttraumatic arthrofibrosis, PLoS One 16 (9) (2021) e0257147.

[12] J. Fertala, et al., Engineering and characterization of the chimeric antibody that targets the C-terminal telopeptide of the alpha2 chain of human collagen I: a next step in the quest to reduce localized fibrosis, Connect. Tissue Res. 54 (3) (2013) 187–196.

[13] A. Steplewski, et al., Blocking collagen fibril formation in injured knees reduces flexion contracture in a rabbit model, J. Orthop. Res. 35 (5) (2017) 1038–1046.

[14] T.T. Wong, A.L. Mead, P.T. Khaw, Prolonged antiscarring effects of ilomastat and MMC after experimental glaucoma filtration surgery, Invest. Ophthalmol. Vis. Sci. 46 (6) (2005) 2018–2022.

[15] P.T. Khaw, et al., Intraoperative and post operative treatment with 5-fluorouracil and mitomycin-c: long term effects in vivo on subconjunctival and scleral fibroblasts, Int. Ophthalmol. 16 (4–5) (1992) 381–385.

[16] L.C. Junqueira, G. Bignolas, R.R. Brentani, Picrosirius staining plus polarization microscopy, a specific method for collagen detection in tissue sections, Histochem. J. 11 (4) (1979) 447–455.

[17] L. Rich, P. Whittaker, Collagen and picrosirius red staining: a polarized light assessment of fibrillar hue and spatial distribution, J. Morpholog. Sci. 22 (2) (2005) 97–104.

[18] A. Steplewski, et al., Auxiliary proteins that facilitate formation of collagen-rich deposits in the posterior knee capsule in a rabbit-based joint contracture model, J. Orthop. Res. 34 (3) (2016) 489–501.

[19] J.E. Jalil, et al., Fibrillar collagen and myocardial stiffness in the intact hypertrophied rat left ventricle, Circ. Res. 64 (6) (1989) 1041–1050.

[20] P.A. Gopinathan, et al., 802980, Study of Collagen Birefringence in Different Grades of Oral Squamous Cell Carcinoma Using Picrosirius Red and Polarized Light Microscopy, vol. 2015, Scientifica, 2015, p. 802980.

[21] L.C. Junqueira, G.S. Montes, E.M. Sanchez, The influence of tissue section thickness on the study of collagen by the Picrosirius-polarization method, Histochemistry 74 (1) (1982) 153–156.

[22] D. Dayan, et al., Are the polarization colors of picrosirius red-stained collagen determined only by the diameter of the fibers? Histochemistry 93 (1) (1989) 27–29.

[23] G.S. Montes, et al., Collagen fibril diameters in arteries of mice. A comparison of manual and computer-aided morphometric analyses, Acta Anat. 135 (1) (1989) 57–61.

[24] I. Allon, et al., Stromal differences in salivary gland tumors of a common histopathogenesis but with different biological behavior: a study with picrosirius red and polarizing microscopy, Acta Histochem. 108 (4) (2006) 259–264.

[25] T.T. Wong, A.L. Mead, P.T. Khaw, Matrix metalloproteinase inhibition modulates postoperative scarring after experimental glaucoma filtration surgery, Invest. Ophthalmol. Vis. Sci. 44 (3) (2003) 1097–1103.

[26] M.J. Baker, et al., Using Fourier transform IR spectroscopy to analyze biological materials, Nat. Protoc. 9 (8) (2014) 1771–1791.

[27] W. Querido, S. Kandel, N. Pleshko, Applications of vibrational spectroscopy for analysis of connective tissues, Molecules 26 (4) (2021).

[28] N.P. Camacho, et al., FTIR microscopic imaging of collagen and proteoglycan in bovine cartilage, Biopolymers 62 (1) (2001) 1–8.

[29] A.C. Jayasuriya, et al., Piezoelectric and mechanical properties in bovine cornea, J. Biomed. Mater. Res. 66 (2) (2003) 260–265.

[30] R. Cheheltani, et al., Fourier transform infrared spectroscopic imaging of cardiac tissue to detect collagen deposition after myocardial infarction, J. Biomed. Opt. 17 (5) (2012) 056014.

[31] A. Steplewski, et al., The impact of cholesterol deposits on the fibrillar architecture of the Achilles tendon in a rabbit model of hypercholesterolemia, J. Orthop. Surg. Res. 14 (1) (2019) 172.

[32] E.P. Paschalis, et al., Spectroscopic characterization of collagen cross-links in bone, J. Bone Miner. Res. 16 (10) (2001) 1821–1828.

[33] D.R. Eyre, M.A. Paz, P.M. Gallop, Cross-linking in collagen and elastin, Annu. Rev. Biochem. 53 (1984) 717–748.

[34] A.J. van der Slot, et al., Elevated formation of pyridinoline cross-links by profibrotic cytokines is associated with enhanced lysyl hydroxylase 2b levels, Biochim. Biophys. Acta 1741 (1–2) (2005) 95–102.

[35] A.J. van der Slot, et al., Increased formation of pyridinoline cross-links due to higher telopeptide lysyl hydroxylase levels is a general fibrotic phenomenon, Matrix Biol. 23 (4) (2004) 251–257.

[36] D. Brickley-Parsons, et al., Biochemical changes in the collagen of the palmar fascia in patients with Dupuytren's disease, J. Bone Joint Surg. Am. 63 (5) (1981) 787–797.

[37] L. Rieppo, et al., Application of second derivative spectroscopy for increasing molecular specificity of Fourier transform infrared spectroscopic imaging of articular cartilage, Osteoarthritis Cartilage 20 (5) (2012) 451–459.

[38] B. Gieroba, et al., Collagen maturity and mineralization in mesenchymal stem cells cultured on the hydroxyapatite-based bone scaffold analyzed by ATR-FTIR spectroscopic imaging, Mater. Sci. Eng. C Mater. Biol. Appl. 119 (2021), 111634.

[39] M. Wilkins, A. Indar, R. Wormald, Intra-operative mitomycin C for glaucoma surgery, Cochrane Database Syst. Rev. 2005 (4) (2005) CD002897.

[40] V.H.X. Foo, et al., Aqueous shunts with mitomycin C versus aqueous shunts alone for glaucoma, Cochrane Database Syst. Rev. 4 (4) (2019) CD011875.

[41] J. Fertala, et al., Target-specific delivery of an antibody that blocks the formation of collagen deposits in skin and lung, Monoclon. Antibodies Immunodiagn. Immunother. 36 (5) (2017) 199–207.

[42] K. Evangelho, C.A. Mastronardi, A. de-la-Torre, Experimental models of glaucoma: a powerful translational tool for the future development of new therapies for glaucoma in humans-A review of the literature, Medicina 55 (6) (2019).

[43] J. Jang, et al., Binding of mitomycin C to blood proteins: a spectroscopic analysis and molecular docking, J. Mol. Struct. 928 (1) (2009) 72–77.

[44] T.R. Cox, et al., LOX-mediated collagen crosslinking is responsible for fibrosis-enhanced metastasis, Cancer Res. 73 (6) (2013) 1721–1732.

[45] N. Ikenaga, et al., Selective targeting of lysyl oxidase-like 2 (LOXL2) suppresses hepatic fibrosis progression and accelerates its reversal, Gut 66 (9) (2017) 1697–1708.

[46] B. Piersma, A. Bank Ruud, Collagen cross-linking mediated by lysyl hydroxylase 2: an enzymatic battlefield to combat fibrosis, Essays Biochem. 63 (3) (2019) 377–387.

[47] M.C. Lampi, C.A. Reinhart-King, Targeting extracellular matrix stiffness to attenuate disease: from molecular mechanisms to clinical trials, Sci. Transl. Med. 10 (422) (2018).

[48] D.J. Tschumperlin, D. Lagares, Mechano-therapeutics: targeting mechanical signaling in fibrosis and tumor stroma, Pharmacol. Ther. 212 (2020), 107575.

[49] M. Walraven, B. Hinz, Therapeutic approaches to control tissue repair and fibrosis: extracellular matrix as a game changer, Matrix Biol. 71–72 (2018) 205–224.